Granular dynamics of cohesive powders in a rotating drum as revealed by speckle visibility spectroscopy and synchronous measurement of forces due to avalanching

H. Yang[1,2], G. L. Jiang[1], H. Y. Saw[3], C. Davies[3], M. J. Biggs[2,4], V. Zivkovic[5]*

1 a. School of Optical-Electrical and Computer Engineering, b. Shanghai Key Lab of Modern Optical System, c. Engineering Research Center of Optical Instrument and System, Ministry of Education , University of Shanghai for Science and Technology, Shanghai, 200093, China

2 School of Chemical Engineering, The University of Adelaide, Adelaide, SA, 5005, Australia

3 Institute of Technology and Engineering, Massey University, Palmerston North, New Zealand

4 School of Science, Loughborough University, LE11 3TU, United Kingdom

5 School of Chemical Engineering and Advanced Materials, Newcastle University, NE1 7RU, United Kingdom

*Corresponding author: Vladimir.Zivkovic@newcastle.ac.uk

ABSTRACT

We have used speckle visibility spectroscopy (SVS) and synchronized force measurements to compare the granular dynamics of two cohesive lactose powders, with Sauter mean diameters of ~29 μm and ~151 μm, in a rotating drum. A load cell (LC) was used to measure forces on the drum mounting frame and enable monitoring of bulk powder motion; SVS is a dynamic light scattering technique particularly suited for studying dynamics in dense, non-ergodic granular systems. Our results reveal that surface slumping and intermittent collisional dynamics in the bulk of the bed are correlated, especially for the fine more cohesive particles (Geldart group C/A boundary), but not as much for the less cohesive larger particles (Geldart group A/B boundary). The specific dissipation energy of the particles in the drum is similar for both powders, and increases linearly with increasing drum speed. However, the dependencies of the load cell and SVS signals on rotation speed have opposing trends for these two powders, indicating different dissipation mechanisms for the different Geldart Groups; collisional dissipation is more important for the Geldart C/A powder, while for the Geldart A/B powder avalanche dissipation is dominant.

Keywords: Granular flow; Rotating drum; Cohesive powders; Avalanches; Jamming; Powder technology.

1. Inroduction

Granular materials and powders in rotating drums are of wide interest not only because of their extensive use in the chemical, minerals, pharmacutical and food processing contexts, but also as model systems in the study of natural disasters, such as avalanches or landslides (Meier et al., 2007; Seiden and Thomas, 2011). Over the previous few decades, the overwhelming majority of the studies of such systems have focused on free-flowing or slightly cohesive materials (Castellanos et al., 1999; Castellanos et al., 2002; Fischer et al., 2008; Jiang et al., 2015; Metcalfe et al., 1995; MiDi, 2004; Orpe and Khakhar, 2007; Zhou and Sun, 2013). However, since many powder materials in nature and industry are substantially cohesive (i.e., inter-particle forces are larger than the particle weight), additional work focusing on cohesive powder flow is highly desirable. Some recent work has examined cohesive granular systems (Chou et al., 2014; Liu et al., 2011; Pignatel et al., 2012; Tegzes et al., 2002, 2003), but these studies have typically used large spherical particles and moisture-induced cohesion.

For many powders, cohesive effects are influenced by other forces besides capillary, such as van der Waals forces, electrostatic or magnetic forces, mechanical interlocking between particles, and combinations of these (McGlinchey, 2005), which lead to flow dynamics different from those observed for moisture-induced cohesion (Alexander et al., 2006; Li et al., 2011; Lumay et al., 2012; Tomas, 2004). In the cohesionless case, it is well known that as the drum rotational speed increases, the granular flow takes on one of a number of regimes such as slumping, rolling, cascading, cataracting, and centrifuging. All of these regimes can be characterized by the angle of repose or flowing speed by imaging techniques (Fischer et al., 2008; MiDi, 2004; Orpe and Khakhar, 2007). In the case of cohesive powders, the behavior of the granular assembly is more complex. In particular, the angle of repose is difficult to measure because of the irregular surface of the flow and the continuous regime does not exist. Indeed, the cohesion induces intermittencies over the whole range of rotational speeds (Alexander et al., 2006; Lumay et al., 2012), and limits the effectiveness of popular imaging techniques.

Davies *et al*. (2002) introduced a load cell device for sensing the motion of particulate material in a rotating cylinder by tracking changes in the centre of gravity of the particle bed, and subsequently demonstrated (Davies et al., 2004) that a load cell could be used to identify the initiation of an avalanche and to track its movement. Later, Alexander *et al.* (Alexander et al., 2006) used this method to compare the experimental flow behaviours of dry glass beads, wet glass beads, and “dry” cohesive powders with the DEM results. They found that dry cohesive powders exhibit history-dependent flow dynamics, significant dilation, and variable avalanche size. Davies and Webster (Davies and Webster, 2010) used the method in experiments with powders from the four different Geldart Groups, and reported distinctive differences in the avalanching behaviour of each group.

Studies of granular dynamics in the bulk region of a rotating drum are very scarce due to limitations of available experimental techniques. Because of strong multiple light scattering, video imaging based optical

velocimetry techniques such as particle image velocimetry (PIV) (du Pont et al., 2005), and particle tracking velocimetry (PTV) (Jain et al., 2002; Warr et al., 1994), are restricted to dilute granular gasses or surface behaviour. Even then, the spatial resolution is not fine enough for them to distiguish collisions between the grains. This limitation holds for other imaging techniques as well, like positron emission particle tracking (PEPT) (Lim et al., 2003; Parker et al., 1997), magnetic resonance imaging (MRI) (Nakagawa et al., 1993; Yamane et al., 1998), and X-ray microtomography (Seidler et al., 2000). Furthermore, none is fast enough to capture the high rates of the micro-collision of grains in the passive bed located in the lower part of the rotating tumbler. By contrast, diffusing-wave spectroscopy (DWS) (Pine et al., 1988), a dynamic light scattering (DLS) technique, can be applied to the study of dense granular media in very small volumes and can resolve the motion of grains over length and time scales of the order of several nanometres and several microseconds respectively (Kim and Pak, 2010; Zivkovic et al., 2009). It is, however, based on temporal correlation functions calculated as a time average, which cannot be used for time-resolved measurements. And in our case, we are interested in the time dependence of collisions between particles.

In this paper, we report a study of the avalanche dynamics of two different lactose powders of different cohesion strengths in a rotating drum, by sychronized measurements with a load cell (LC) and speckle visibility spectroscopy (SVS). SVS is able to measure time-resolved collisional motion of grains in dense systems with fine spatio-temporal resolution (Bandyopadhyay et al., 2005), which we have previously used to measure the intermittent avalanches on the surface of granular flow in a rotating drum (Yang et al., 2015). The experimental details of both techniques are introduced first, followed by a results section where both LC and SVS results are presented separately for two Geldart group powders followed by section with comparison of the results for these two powders.

2. Experimental details

2.1 Drum system

The results reported in this work are obtained in a drum with an inner diameter of 200 mm and length of 300 mm, as depicted schematically in Fig. 1. The drum, has a front face-plate of clear transparent perspex to permit optical access and cylindrical walls of semi-transparent perspex; it was half-filled with granular material and placed on a pair of rollers turned by a DC motor at rotation rates in the range 3-25 revolutions per minute (RPM). A white tape 12 mm wide and 100mm long was stuck on the front face-plate as a reference flag for the jamming state of a powder in a SVS signal. The points A, B, and C on the profile of the granular material, as shown in Fig. 1., are the spot points used in this SVS study.

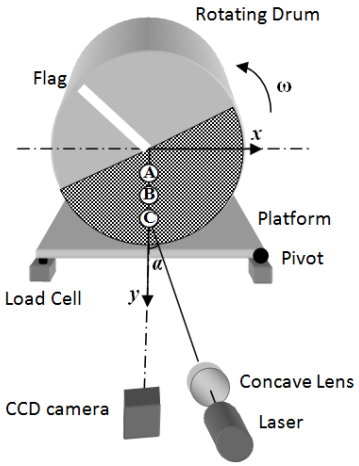

Fig. 1 Schematic diagram of the experimental setup, showing the spot points, A ($x = 0$ mm, $y = 15$ mm), B ($x = 0$ mm, $y = 25$ mm), and C ($x = 0$ mm, $y = 35$ mm).

2.2 Granular material

The granular materials used in this study were two model milled lactose powders with size distribution parameters given in Table 1 (Saw et al., 2013a); also shown are surface-volume diameter, d_{32}, loose poured bulk density, ρ_B, and cohesion for the condition of zero preconsolidation stress, C_0, which was obtained from shear cell measurements (Saw et al., 2013b) following the approach outlined by Saw *et al.* (Saw et al., 2013a); the particle density of lactose is 1540 kg m^{-3}. Note that the size distribution parameters were found using data obtained with a Malvern Mastersizer 2000, using bins equivalent to a full sieve analysis according to BS410 (British Standards Institution, 2000). The finer powder, termed powder CA, lies close to the C/A boundary in the Geldart Classification (Geldart, 1973); the other powder, termed powder AB, lies on the A/B boundary. In tests in an 80 mm diameter gas fluidized bed, powder CA could not be fluidized, while powder AB was relatively easy to fluidize.

Tab. 1 Particle Properties

Powder	d_{10} µm	d_{50} µm	d_{90} µm	d_{32} µm	ρ_B kg m^{-3}	C_0 kPa
CA	7.3	34.5	85.3	28.9	441.5	0.0534
AB	88.6	257.0	538.4	150.8	802.7	0.0245

2.3 SVS

Speckle visibility spectroscopy (Bandyopadhyay et al., 2005) involves illuminating the target material, in this work a granular solid, with a monochromatic laser light beam of wavelength λ, as shown schematically in Fig. 1. The photons emerge from the granular material after diffusing within it, to form a speckle pattern that is detected by a CCD camera in the far field. In the absence of any motion of the light scatterers (the particles here), each pixel detects a constant intensity as illustrated by an example in Fig 2(a). Motion of the scatterers leads, however, to temporal fluctuations over the pixels. For a given exposure time, the faster the dynamics of the grains, the more the speckle image is blurred and the speckle image possesses less contrast; this enables the capture of rapid changes in the granular material during an un-jamming event with elevated levels of interparticle collisions in the bulk of the drum as illustrated in Fig. 2 (b). This variation in intensity can be quantified by the variance of the intensity (Bandyopadhyay et al., 2005)

$$V_2(T) \propto \langle I^2 \rangle_T - \langle I \rangle^2 \tag{1}$$

where $\langle \cdots \rangle_T$ denotes the average over pixels exposed for a duration *T*. The proportionality constant of $V_2(T)$ is set by the laser intensity and the ratio of speckle to pixel size (*i.e.* it is set-up dependent). It can, however, be eliminated by considering the variance ratio $V_2(2T)/V_2(T)$. For diffusely backscattered light from particles moving with random ballistic motion, the theory of SVS (Bandyopadhyay et al., 2005) gives the variance ratio as

$$\frac{V_2(2T)}{V_2(T)} = \frac{e^{-4\Gamma T} - 1 + 4\Gamma T}{4(e^{-2\Gamma T} - 1 + 2\Gamma T)} \tag{2}$$

where $\Gamma = 4\pi\delta v/\lambda$. The root mean fluctuation in the speed of the particles, $\delta v = \sqrt{\langle \delta v^2 \rangle}$, which is equal to the collision velocity and related directly to the so-called granular temperature (Ogawa, 1978), can be obtained by inverting Eq. 2, as illustrated in Fig. 2 (c). The fluctuation speed that can be detected with a particular experimental set-up is dictated by the wavelength of the light used and the scan speed of the CCD camera. This makes the approach ideal for probing in detail interparticle collisions during un-jamming events in the so-called passive layer in the lower part of the rotating drums (Yang et al., 2015). Note that the value of the velocity fluctuations, $\langle \delta v^2 \rangle^{1/2}$, for the jammed grains is the same as that of the flag signal, although the grey-scale values of these two events are different as shown in Fig. 2(b). Thus, SVS measurements enable jamming (solid body dynamics) events to be easily distinguished from un-jamming (fluid-like granular collisional dynamics) events

In the SVS experimental setup used here, the laser is of wavelength λ=532 nm and power 300 mW (Torus 300, Laser Quantum, UK). The laser beam was passed through a concave lens and an aperture before illuminating normally onto the end of the drum in a spot of around 10 mm diameter (points A, B or C in Fig. 1). A line scan CCD camera (Spyder3, DALSA, Canada) of 1024 pixels, each $14\ \mu m \times 14\ \mu m$ and 8-bits deep, was placed about 350 mm away, with its optical axis normal to the drum, such that the ratio of pixel to speckle size is about 0.5. A polarizer, whose direction was vertical to that of the incident laser, was used to block the light from single scattering events. A line filter was used on the CCD camera to eliminate the ambient light. Therefore, the signal originates from multiple scattered incident photons and the measured fluctuation velocity is an ensemble average over an interior region several particles deep from the side walls (Bandyopadhyay et al., 2005). The camera was operated at a frame rate of 20 kHz, giving a sample time $T = 50\mu s$, and the laser power was adjusted to give an average grey scale level of 50. Each measurement for a particular condition (i.e. point/drum speed) involved collecting video data for 1000 seconds.

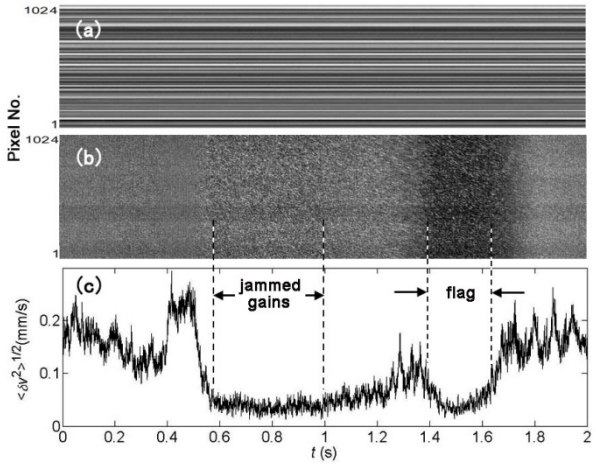

Fig. 2 Example of SVS results and analysis for powder CA in the drum at point A: (a) intensity across the CCD pixels *vs.* time when the drum is stationary; (b) intensity across the CCD pixels *vs.* time when a flag signal appears during two avalanche events at a rotational speed of 3 RPM; (c) root-mean-particle fluctuation velocity, $\langle \delta v^2 \rangle^{1/2}$, evaluated from the data in (b).

2.4 Load Cell

The load cell device for characterizing the dynamics of avalanches of granular materials in rotating drums is scematically shown in Fig. 3 and previously described in detail by Davies *et el* (Davies et al., 2002; Davies et al., 2004). The magnitude of avalanches is characterized by measuring the shift in the centre of gravity of the powder

bed as it avalanches within a rotating drum. As avalanches take place, the shift in the centre of gravity of the powder bed alters the distribution of forces between the pivot and the load cell. The weight variations recorded by the load cell are the combined effects of avalanche size and total displacement. The data was filtered with a Bartlett window band pass convolution filter. The low frequency cut off is 0.1 Hz and the high frequency cut off is 10 Hz. Fig. 3 shows a series of discrete avalanches of powder CA recorded by the load cell at rotational speed of 3 rpm; the signal, w_n, is normalised with respect to the weight of material in the drum. Slumping, the periodic traversing movement of bulk volumes of powder in the surface layers relative to the powder bed in the lower part of the drum, starts when the powder bed fractures under the influence of gravitational forces when the angle of the bed to the horizontal increases. As the powder bulk is redistributed, the centre of gravity of the whole powder mass in the drum changes. Slumping is recorded as the rising curve, and at the end of slumping which can comprise multiple events, all the powder in the drum is lifted as a solid body, which is recorded as the quickly declining curve. The process then repeats.

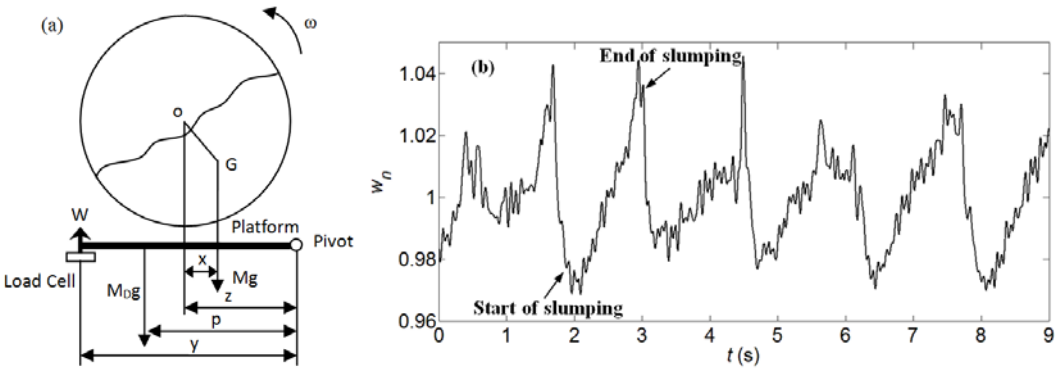

Fig.3 (a) Schematic diagram of moments arising from powder bed, dead weight of system and load cell reaction. (b) An example of normalized weight signal, w_n, for powder CA at rotating speed of 3 rpm with indicated start and end of slumping.

3. Results and Analysis

3.1 Powder CA

Fig. 4 shows the synchronised normalized weight, w_n, and velocity fluctuations, $\langle \delta v^2 \rangle^{1/2}$, at the point A at 3 RPM for rotating drum filled with powder CA. It is clear that during the elevation of the bed (*i.e.* decline of normalized weight), the particle velocity fluctuation, $\langle \delta v^2 \rangle^{1/2}$, is almost zero and very close to the flag signal (as shown in Fig. 2(c)) indicating solid body dynamics (no relative movement and collisions of the grains). Once slumping occurs as indicated in the normalized weight signal, the collisions among the grains also occur frequently which results in the rising of the value of $\langle \delta v^2 \rangle^{1/2}$ as can be seen in Fig. 4. We will refer to these peaks in SVS signals as un-jamming events in the rest of the paper. Both load cell and SVS

measurement indicated quite periodic signals albeit with some irregularities. Furthermore, the peaks in SVS signals are not synchronized with LC signal usually dropping first followed quickly by load cell signal drop. However, it is difficult to determine if the start of slumping and un-jamming events in drum body are perfectly correlated due to high noise in both SVS and load cell measurements and low signal strength of the raw data.

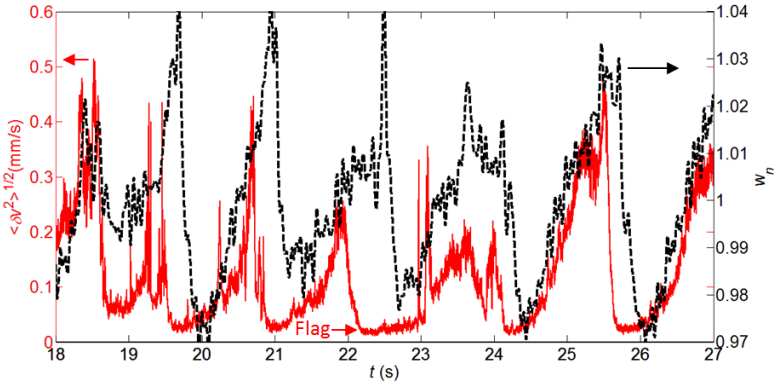

Fig. 4. (colour online) Sample of synchronised normalized weight (black dash) and particle velocity fluctuations, $\langle \delta v^2 \rangle^{1/2}$, (grey, red online) for the point A at rotating speed of 3 rpm using powder CA.

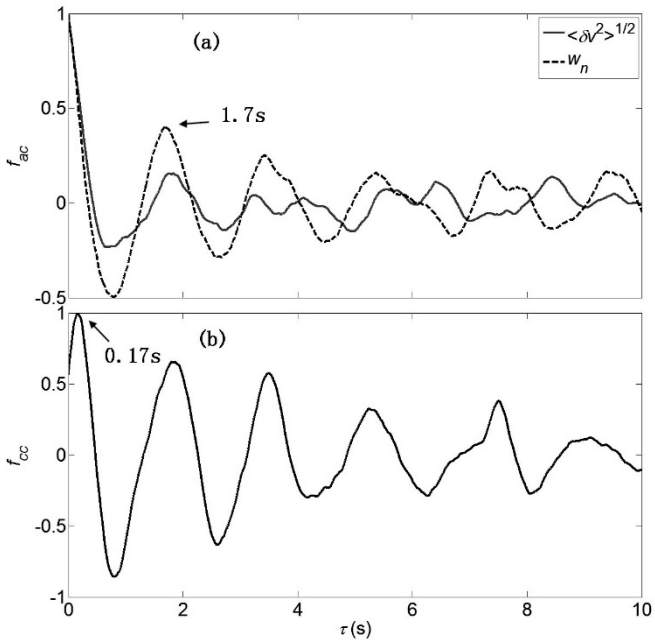

Fig. 5 (a) The normalized auto-correlation function, f_{ac}, of $\langle \delta v^2 \rangle^{1/2}$ (red solid line) and w_n (black dash line), (b) the normalized cross correlation function, f_{cc}, between $\langle \delta v^2 \rangle^{1/2}$ and w_n for the point A at 3 rpm using powder CA.

In order to characterize the periodicity of the slumping and un-jamming events as measured respectively by LC and SVS technique, we calculate the auto-correlation and cross-correlation of these two signals. Fig. 5(a) shows the normalized auto-correlation function, f_{ac}, of $\langle \delta v^2 \rangle^{1/2}$ and w_n with the lag time, τ, indicating that

both slumping (w_n) and un-jamming processes ($\langle \delta v^2 \rangle^{1/2}$) are quite periodic with almost the same period of 1.7 s. Whilst in the load cell data auto-correlation function second and third harmonics are quite pronounced, the SVS signal does not show such high periodicity, as higher harmonics are not easily distinguishable. Moreover, the cross-correlation curve, shown in Fig. 5(b), indicates that there is a typical lag time, $\tau_0 = 0.17\ s$, between the SVS and load cell signals. It seems likely this originates from the difference in the signals' maxima, where the SVS curve typically drops a little earlier than the load curve record with the reported lag time. Although we cannot be certain if the same time lag applies for the signal rise due to noise and low level signals, logically it would be possible. If that is true, these results would be experimental evidence of the deformation of the granular bed with corresponding un-jamming events starting before the avalanche, inline with the DEM and diffusive wave spectroscopy (DWS) results in similar granular systems (Amon et al., 2013; De Richter et al., 2012; Liu et al., 2011).

Fig. 6 shows the comparison time traces of the particle velocity fluctuations, $\langle \delta v^2 \rangle^{1/2}$, at rotation speeds of 3, 10, and 25 RPM for the point A using powder CA. The peak heights and distance between successive peaks in the SVS signals are similar at all speeds, but the period of these un-jamming events decreases with increasing rotational speed. Consequently, the bulk of the bed at higher speeds is rarely completely jammed as can be seen in Fig. 6, but the low level base values indicate intermittent dynamics with jamming and un-jamming events occurring successfully.

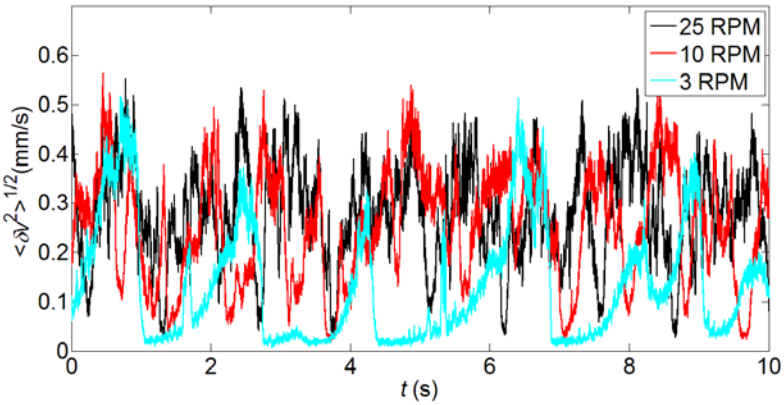

Fig. 6 Particle velocity fluctuations, $\langle \delta v^2 \rangle^{1/2}$, at 3 RPM (light gray, cyan online), 10 RPM (gray, red online), and 25 RPM (black) for the point A using powder CA.

Fig. 7(a) shows that the avalanching period, *T*, decreases exponentially with increasing of rotation speed and becomes almost constant after 15 RPM. Fig. 7(b) shows the variation of $\langle \delta v^2 \rangle^{1/2}$ and the standard deviation of normalized weight, σ_{w_n} proportional to the size of avalanche, for powder CA particles as a function of the rotational speed. It indicates that the granular temperature of CA particles increases with the rotating speed and becomes constant for rotational speeds above about 15 rpm, which agrees with the trends for avalanching period and previous work by Davies and Webster (Davies and Webster, 2010). Comparison of both signals

clearly indicates that the variation of $\langle \delta v^2 \rangle^{1/2}$ with the RPM is consistent with that of the standard deviation of normalized weight.

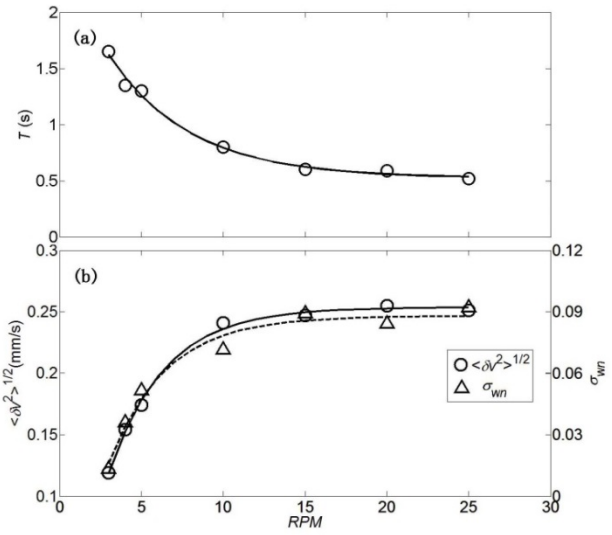

Fig. 7 (a) The period of avalanche, *T*, (b) the variation of the particle velocity fluctuations, $\langle \delta v^2 \rangle^{1/2}$, (circle) for the point A and the standard deviation of normalized weight, σ_{w_n}, (triangle) with the rotating speeds for powder CA. The solid line and the dashed line represent the best exponential fit to the data.

Fig. 8 shows the comparison of the time resolved $\langle \delta v^2 \rangle^{1/2}$ of CA particles for the point A, B and C at 3 *RPM*. It is clear that the granular temperature is largest for point A and smallest for point C, i.e. decreases with the depth, which is consistent with previous results that the granular temperature profile along the sidewall decays with depth (Boateng and Barr, 1997; De Richter et al., 2012; Jain et al., 2002; Katsuragi et al., 2010). We determined the same trend for all studied rotational speeds as can be seen in Fig. 9(a), although the difference increases with increasing speed. The trend for time lag spatial dependence is not very clear as can be seen in Fig. 9(b). However, it seems that jamming usually starts first at point C, the deepest point, but at high speeds this trend reverses as the SVS signal stops after the load cell signals, at least for points B and C, in contradiction with previous lag trend. Due to noise in the data, further studies would be needed to elucidate this change in trend further.

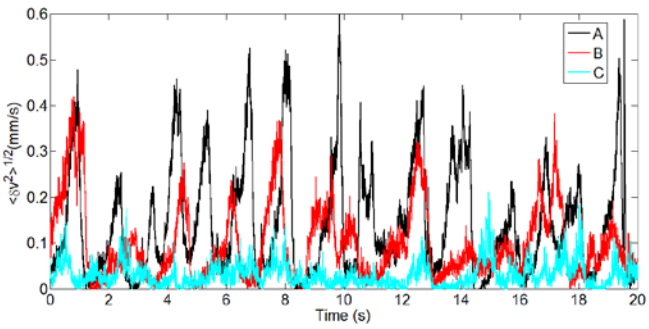

Fig. 8 (color online) Comparison of the time resolved particle velocity fluctuations, $\langle \delta v^2 \rangle^{1/2}$, of powder CA particles for the point A, B and C (separate un-synchronized measurements) at 3 *RPM*.

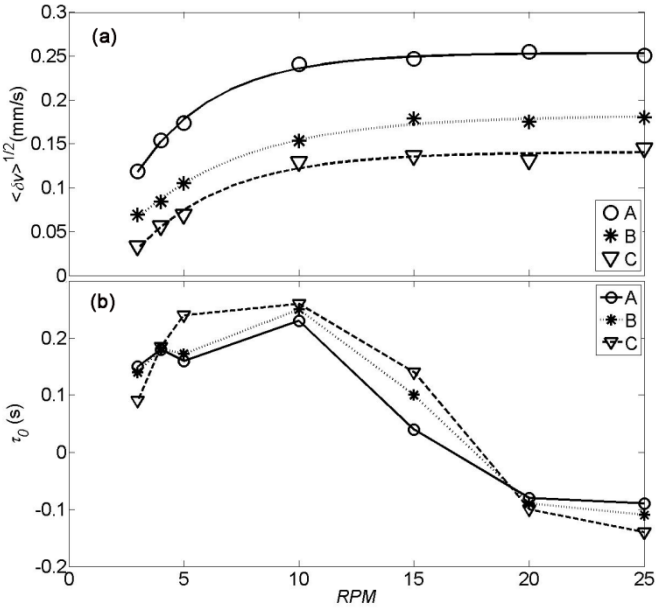

Fig. 9 The variation of (a) $\langle \delta v^2 \rangle^{1/2}$ and (b) lag time, τ_0, with the rotational speed for the point A, B and C, for powder CA.

3.2 Powder AB

Fig. 10 shows the synchronised normalized weight, w_n, and $\langle \delta v^2 \rangle^{1/2}$ for the point A at 3 rpm with powder AB which is less cohesive than powder CA. It is immediately evident that both signals are more irregular and have more noise in comparison with measurements on CA particles. A direct consequence of this is that the periodicity of both signals as well as the cross-correlation of these two signals is less obvious in raw signal plots. Yet, there are notable peaks in auto-correlation of both signals at around 2 s with a particularly distinct peak at 1.9 s in the normalised weight signal as shown in Fig. 11(a). Higher harmonics are not as prominent, and sub-harmonics are present in both load cell and SVS auto-correlation signals unlike the powder CA measurements. This is probably a consequence of more fluid-like behaviour in the bulk of the bed as indicated in SVS signal. Direct comparison of the bottom of the $\langle \delta v^2 \rangle^{1/2}$ signal with the flag signal shows clearly that the grains are not absolutely jamming during the elevation of the drum. Figure 12 shows photographs of profiles for both the CA and AB powders. In contrast to CA, while powder AB does not show a completely horizontal free surface, an indicator of a permanent region of fluidization (Castellanos et al., 2002; Huang et al., 2010), there is some indication of partial fluidization by gas entrained into the bulk powder during the

avalanching process as contemplated by Castellanos *et al.* (Castellanos et al., 2002). Cross-correlation of the load cell and SVS signals has a maximal peak at around 0.6 s but once again there are many more significant peaks and sub-peaks indicating that the two signals are not completely correlated. This would indicate that the micro-dynamics in the bulk of the drum is not completely synchronized with the avalanching of the surface layer.

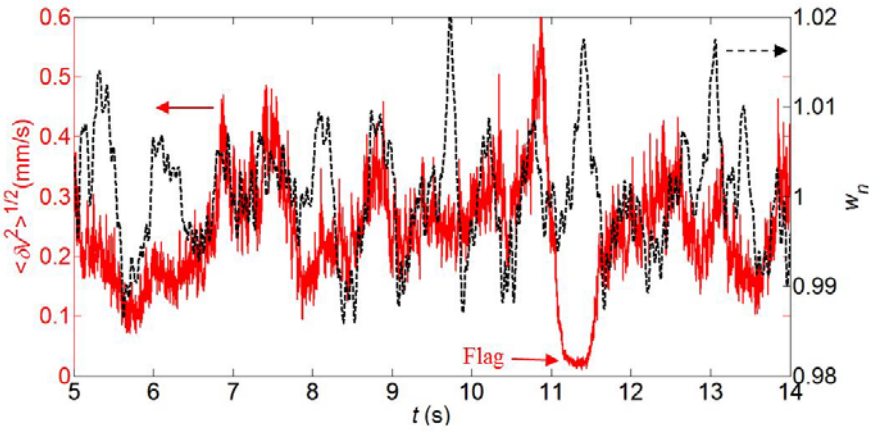

Fig. 10. (colour online) Sample of synchronised normalized weight (black dash) and $\langle \delta v^2 \rangle^{1/2}$ (grey, red online) for the point A at 3 rpm using powder AB.

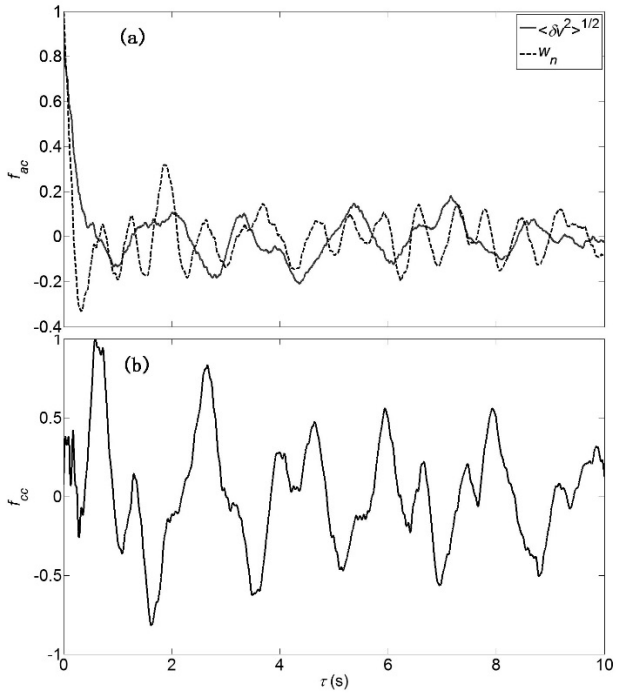

Fig. 11. Evaluation of (a) the normalized auto-correlation function, f_{ac}, of $\langle \delta v^2 \rangle^{1/2}$ (red solid line) and w_n (black dash line), (b) the normalized cross correlation function, f_{cc}, between $\langle \delta v^2 \rangle^{1/2}$ and w_n, for the point A at 3 rpm using powder AB.

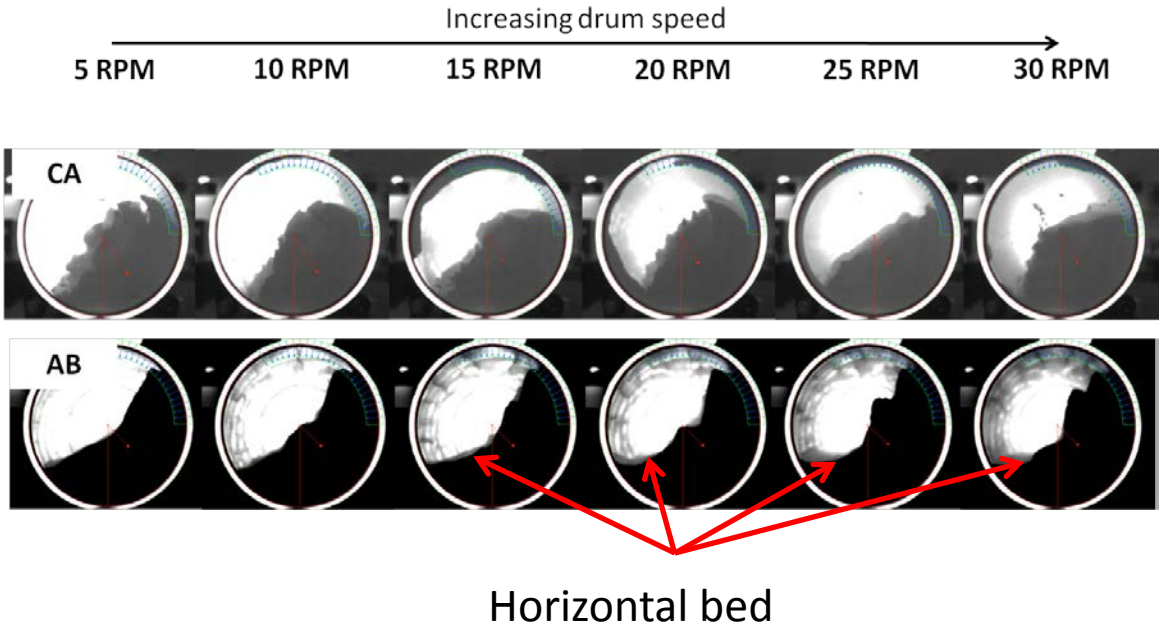

Fig. 12. Backlit photographs of the front face during avalanching for powders CA and AB, showing surface profiles.

Fig. 13 shows the comparison of the particle velocity fluctuations, $\langle \delta v^2 \rangle^{1/2}$, at the rotational speeds of 3, 10, and 25 RPM for the point A using powder AB. It is can be seen that the collisional dynamics intensity (granular temperature) increases with increasing rotation speed, which is different from observations for the CA powder as shown in Fig. 6.

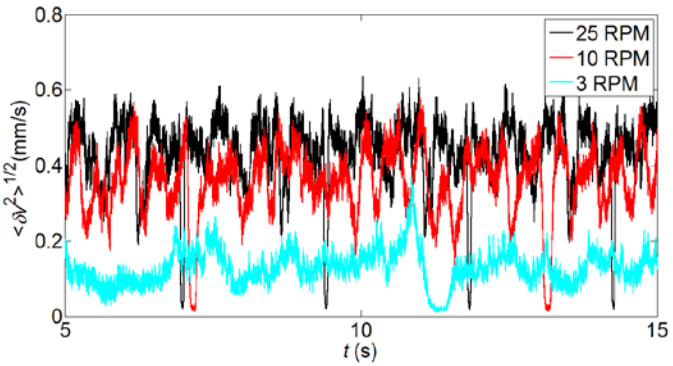

Fig. 13 Comparison of the particle velocity fluctuations, $\langle \delta v^2 \rangle^{1/2}$, at 3 RPM (light gray, cyan online), 10 RPM (gray, red online), and 25 RPM (black) for the point A using powder AB.

Fig. 14(a) shows that the avalanching period, *T*, decreases exponentially with increasing rotational speed. A notable difference from results for the CA particles as shown in Fig. 7(a) is that the period of powder AB does not level and keeps decreasing with drum speed even after 15 RPM. Fig. 14(b) shows the variation of the

average of $\langle \delta v^2 \rangle^{1/2}$ and the standard deviation of normalized weight, σ_{w_n}, of AB with increasing rotational speed. It indicates that the size of powder AB avalanches keeps increasing with the rotational speed in contrast to the avalanching behaviour of powder CA as shown in Fig. 7(b). Furthermore, the $\langle \delta v^2 \rangle^{1/2}$ also increases with rotational speed, and the data for $\langle \delta v^2 \rangle$ is linearly dependent with RPM as shown in the inset of Fig. 14(b).

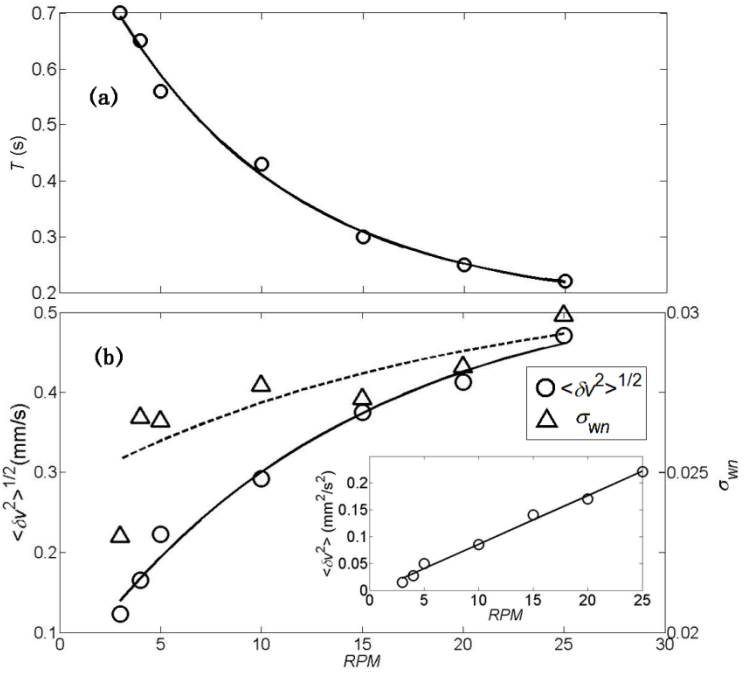

Fig. 14 (a) The period of an avalanche, *T*, (b) the variation of $\langle \delta v^2 \rangle^{1/2}$ (circle) for the point A and the standard deviation of normalized weight, σ_{w_n}, (triangle) for powder AB *vs* the rotation speed. The solid and dashed lines are a guide to the eye only. The inset in (b) shows $\langle \delta v^2 \rangle$ (circle) *vs* the rotational speed with the linear fitting line.

Fig. 15 shows the comparison of the time resolved $\langle \delta v^2 \rangle^{1/2}$ of AB particles for the point A, B and C at 3 *RPM*. It is clear that the granular temperature is biggest for point A which is same result as for the CA particles. However, with reference to Fig. 8 which shows data for powder CA, it is seen that peak heights for AB particles decrease much faster with the depth than those for CA particles; indeed for the deepest point C the peaks for AB almost vanish completely. This indicates that the influence of surface avalanching on bulk granular dynamics decreases with depth as already hinted by lack of strong correlation between SVS and LC signal. We determined the same trend for all studied rotational speeds as can be seen in Fig. 16, although the relative difference increases with rotational speed.

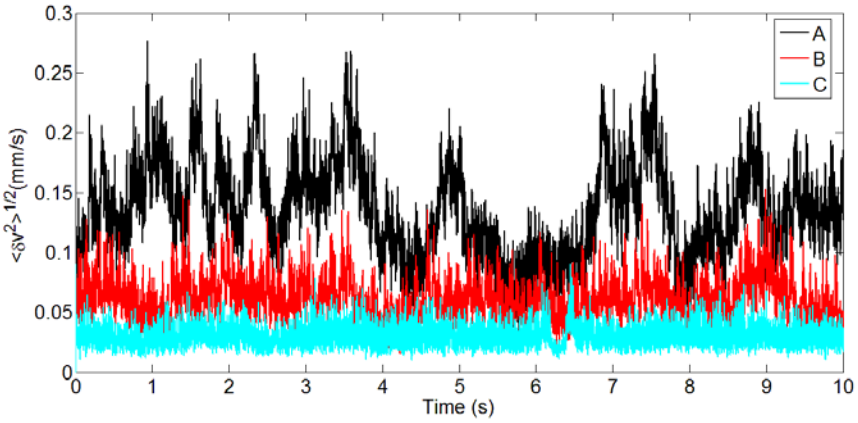

Fig. 15 (color online) Comparison of the time resolved particle velocity fluctuations, $\langle \delta v^2 \rangle^{1/2}$, of powder AB particles for the point A, B and C (separate un-synchronized measurements) at 3 *RPM*.

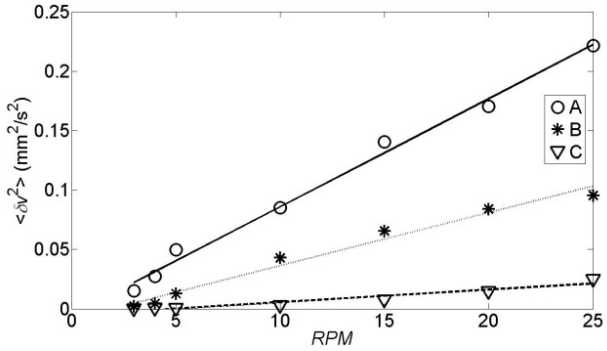

Fig. 16 The variation of $\langle \delta v^2 \rangle$ with rotational speed for spot points A, B and C, for powder AB particles.

3.3 Comparison of CA with AB

Fig. 17 shows the comparison of the time resolved particle velocity fluctuations, $\langle \delta v^2 \rangle^{1/2}$, of AB particles with those of CA particles at 3 RPM. It seems that the bulk of the granular medium of AB particles is almost continuously fluidized and as such not completely correlated with surface avalanches like for more cohesive particles (CA) which are not fluidized in the bulk of the drum.

Fig. 18(a) shows the comparison of the variation of the standard deviation of normalized weight of CA (circle) and that of AB (triangle) particles as a function of the rotational speed. It is clear that the σ_{w_n} of AB is almost constant with increasing rotational speed compared with that of CA which increases before leveling at approximately 10 RPM.. This result is consistent with the results by Davies and Webster (2010) that the Geldart group of the powders can be indicated by the variance of the load cell signal of the powder in the

rotating drum.

Fig. 18(b) shows that the average of $\langle \delta v^2 \rangle$ of AB is higher than that of CA, which is in agreement with discrete element modelling results by Liu *et al.* (Liu et al., 2011) (*i.e.* $\langle \delta v^2 \rangle$ decreases with the cohesion). Interestingly, the comparison of the variation of the average of $\langle \delta v^2 \rangle$ of the two powders from different Geldart groups shows two distinctly different trends. The square of fluctuation velocity of AB particles increases linearly with the RPM, whilst for CA particles, the granular temperature increases at lower RPM and becomes constant at higher RPM (above 15 RPM). Thus, in the bed at the bottom of the drum the particles of these two powders from different Geldart Groups exhibit different behaviours, and to the authors' knowledge, this has not been previously reported.

Fig. 18 (c) shows that the product of $\sigma_{w_n} \cdot \langle \delta v^2 \rangle$ for AB and CA particles is roughly the same size and increases with the RPM almost linearly, particularly for AB particles. This suggests that crudely, these two indicators of dissipation mechanism, avalanche size and collisional dissipation, are proportional to the inputted energy (*i.e. RPM*). Furthermore, this indicates that dissipation pathways are different for AB and CA and that for very cohesive particles collisional dissipation (*i.e.* granular temperature) is more important. Although the frictional dissipation is not directly measured, our results of jamming in the drum bulk would indicate this is very important at lower rotational speed especially for CA powders (see for example Figure 17).

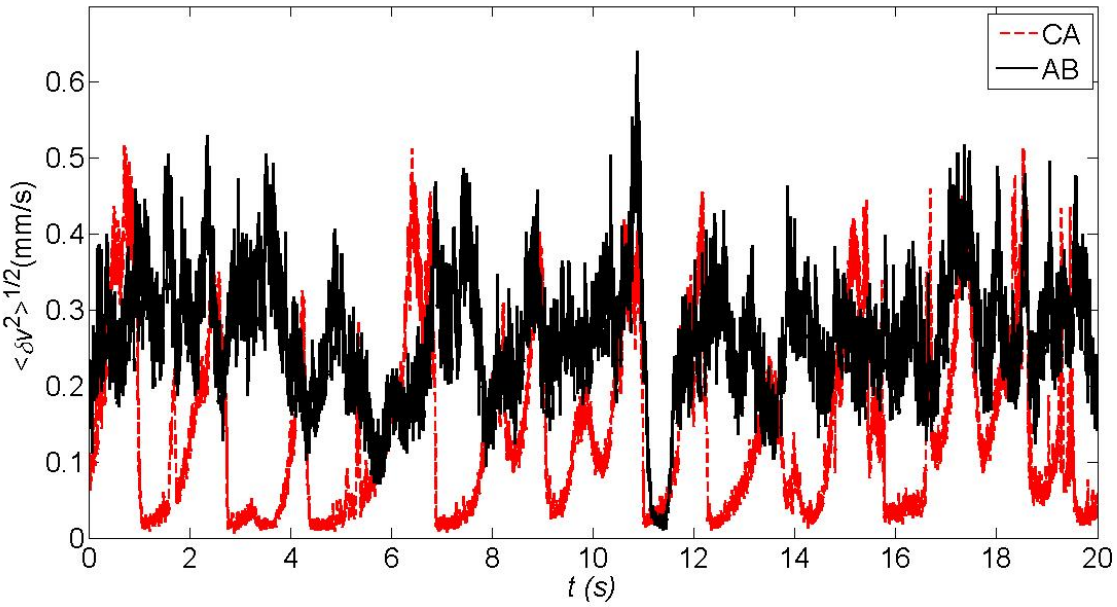

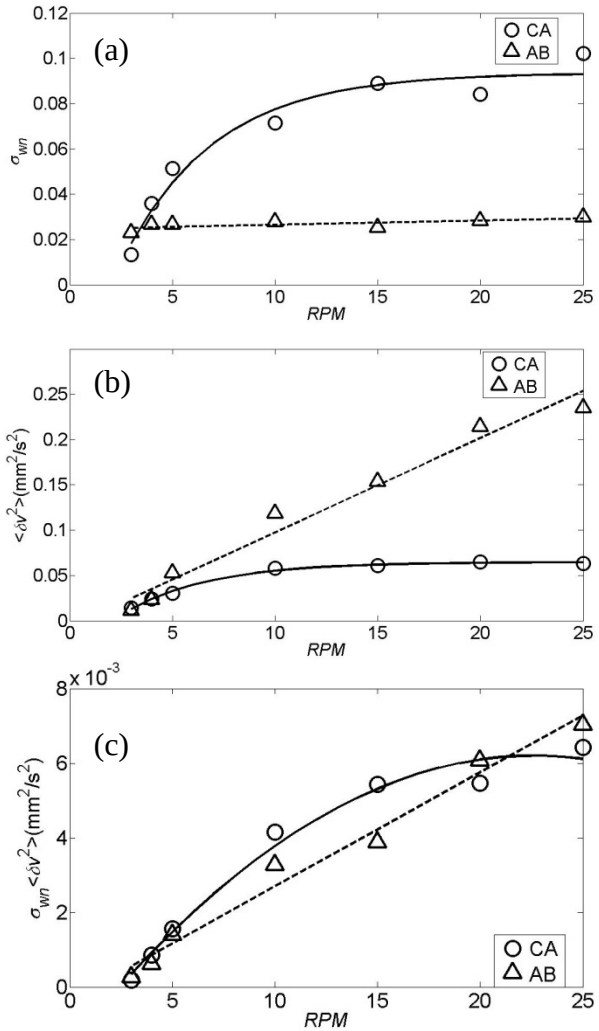

Fig. 17 (color online) Comparison of the time resolved particle velocity fluctuations, $\langle \delta v^2 \rangle^{1/2}$, of AB (black) with that of CA (gray dash, red online) particles at 3 RPM, for point A.

Fig. 18 Comparison of the variation of (a) the standard deviation of normalized weight, σ_{w_n}, (b) the $\langle \delta v^2 \rangle$ for the point A, and (c) the product of $\sigma_{w_n} \cdot \langle \delta v^2 \rangle$ with rotational speed, for powder CA (circle) and powder AB (triangle).

Conclusion

In this paper we have used force measurements with a synchronized load cell (LC) and speckle visibility

spectroscopy (SVS) to compare the granular dynamics of two cohesive lactose powders, one lying close to the Geldart C/A boundary (powder CA), and the other lying close to the Geldart A/B boundary (powder AB) in a rotating drum. Our results reveal that for the more cohesive powder CA, the surface slumping and intermittent collisional dynamics in the bulk of the bed are highly correlated; un-jamming occurs during slumping while the bed is jammed during elevation of the bed, while this correlation is dampened for the less cohesive AB powder due to almost permanent fluidization in the bulk of the bed. We have confirmed that for the less cohesive Geldart group A/B powder the avalanche magnitude increases with drum speed, but for the Geldart group CA powder there is a typical avalanche magnitude independent of the rotating speed as revealed by load cell measurements. SVS measurements determined two discriminating essentially opposite trends to load cell measurements; granular temperature increased linearly with drum speed for AB powder whilst it plateaued for the more cohesive CA powder. Interestingly the product of the standard deviation of the force signal due to the motion of the bulk powder, obtained by a load cell (LC) , and the SVS signal pertaining to the motion of individual particles, increases linearly with rotational speed, i.e. it is proportional to the energy input. The synchronous use of load cell measurements and the SVS technique is a good indicator of the avalanche magnitude and collisional dissipation as two distinct dissipation mechanisms in a rotating drum. Collisional dissipation is the dominant mechanism for very cohesive particles in rotating drums showing the bulk collisional dynamics to be even more important in this case although rarely studied.

ACKNOWLEDGEMENTS

This work has been supported by National Natural Science Foundation of China (11572201), Innovation Program of Shanghai Municipal Education Commission (15ZZ072), Hujiang Foundation of China (C14002).

Reference

Alexander, A.W., Chaudhuri, B., Faqih, A., Muzzio, F.J., Davies, C., Tomassone, M.S., 2006. Avalanching flow of cohesive powders. Powder Technology 164, 13-21.

Amon, A., Bertoni, R., Crassous, J., 2013. Experimental investigation of plastic deformations before a granular avalanche. Physical Review E 87, 012204.

Bandyopadhyay, R., Gittings, A.S., Suh, S.S., Dixon, P.K., Durian, D.J., 2005. Speckle-visibility spectroscopy: A tool to study time-varying dynamics. Review of Scientific Instruments 76, 093110.

Boateng, A.A., Barr, P.V., 1997. Granular flow behaviour in the transverse plane of a partially filled rotating cylinder. Journal of Fluid Mechanics 330, 233-249.

British Standards Institution, 2000. BS 410-1:2000. Test sieves. Technical requirements and testing. Test sieves of metal wire cloth.
Castellanos, A., Valverde, J.M., Pérez, A.T., Ramos, A., Watson, P.K., 1999. Flow regimes in fine cohesive powders. Physical review letters 82, 1156.
Castellanos, A., Valverde, J.M., Quintanilla, M.A.S., 2002. Fine cohesive powders in rotating drums: Transition from rigid-plastic flow to gas-fluidized regime. Physical Review E 65, 061301.
Chou, H.T., Chou, S.H., Hsiau, S.S., 2014. The effects of particle density and interstitial fluid viscosity on the dynamic properties of granular slurries in a rotating drum. Powder Technology 252, 42-50.
Davies, C., Webster, E.S., 2010. Geldart group indication from powder measurements with a rotating drum instrument, in: Kim, S.D., Kang, Y., Lee, J.K., Seo, Y.C. (Eds.), The 13th International Conference on Fluidization - New Paradigm in Fluidization Engineering. ECI Symposium Series, Gyeong-ju, Korea.
Davies, C.E., Tallon, S.J., Fenton, K., Brown, N., Petersen, M., 2002. Direct Sensing of the Motion of Solids in Slowly Rotating Cylinders, World Congress on Particle Technology 4 Sydney, Australia.
Davies, C.E., Tallon, S.J., Fenton, K., Brown, N., Williams, A., 2004. A New approach to monitoring the movement of particulate material in rotating drums. Developments in Chemical Engineering and Mineral Processing 12, 263-275.
De Richter, S.K., Le Caër, G., Delannay, R., 2012. Dynamics of rearrangements during inclination of granular packings: the avalanche precursor regime. Journal of Statistical Mechanics: Theory and Experiment 2012, P04013.
du Pont, S.C., Fischer, R., Gondret, P., Perrin, B., Rabaud, M., 2005. Instantaneous velocity profiles during granular avalanches. Physical review letters 94, 048003.
Fischer, R., Gondret, P., Perrin, B., Rabaud, M., 2008. Dynamics of dry granular avalanches. Physical Review E 78, 021302.
Geldart, D., 1973. Types of gas fluidization. Powder Technology 7, 285-292.
Huang, Q., Zhang, H., Zhu, J., 2010. Onset of an innovative gasless fluidized bed—comparative study on the fluidization of fine powders in a rotating drum and a traditional fluidized bed. Chemical Engineering Science 65, 1261-1273.
Jain, N., Ottino, J.M., Lueptow, R.M., 2002. An experimental study of the flowing granular layer in a rotating tumbler. Physics of Fluids 14, 572-582.
Jiang, Y.-J., Zhao, Y., Towhata, I., Liu, D.-X., 2015. Influence of particle characteristics on impact event of dry granular flow. Powder Technology 270, 53-67.
Katsuragi, H., Abate, A.R., Durian, D.J., 2010. Jamming and growth of dynamical heterogeneities versus depth for granular heap flow. Soft Matter 6, 3023-3029.
Kim, K., Pak, H.K., 2010. Diffusing-wave spectroscopy study of microscopic dynamics of three-dimensional granular systems. Soft Matter 6, 2894-2900.
Li, S., Marshall, J.S., Liu, G., Yao, Q., 2011. Adhesive particulate flow: The discrete-element method and its application in energy and environmental engineering. Progress in Energy and Combustion Science 37, 633-668.
Lim, S.Y., Davidson, J.F., Forster, R.N., Parker, D.J., Scott, D.M., Seville, J.P.K., 2003. Avalanching of granular material in a horizontal slowly rotating cylinder: PEPT studies. Powder Technology 138, 25-30.
Liu, P.Y., Yang, R.Y., Yu, A.B., 2011. Dynamics of wet particles in rotating drums: effect of liquid surface tension. Physics of Fluids (1994-present) 23, 013304.

Lumay, G., Boschini, F., Traina, K., Bontempi, S., Remy, J.C., Cloots, R., Vandewalle, N., 2012. Measuring the flowing properties of powders and grains. Powder Technology 224, 19-27.
McGlinchey, D., 2005. Bulk property characterisation, in: McGlinchey, D. (Ed.), Characterisation of Bulk Solids. CRC Press, Blackwell Publishing Oxford, pp. 48-84.
Meier, S.W., Lueptow, R.M., Ottino, J.M., 2007. A dynamical systems approach to mixing and segregation of granular materials in tumblers. Advances in Physics 56, 757-827.
Metcalfe, G., Shinbrot, T., McCarthy, J.J., Ottino, J.M., 1995. Avalanche mixing of granular solids.
MiDi, G.D.R., 2004. On dense granular flows. The European Physical Journal E 14, 341-365.
Nakagawa, M., Altobelli, S.A., Caprihan, A., Fukushima, E., Jeong, E.K., 1993. Non-invasive measurements of granular flows by magnetic resonance imaging. Experiments in fluids 16, 54-60.
Ogawa, S., 1978. Multitemperature theory of granular materials, in: Satake, S.C.C.M. (Ed.), Proceedings of the US–Japan seminar on continuum mechanical and statistical approaches in the mechanics of granular materials. Gakajutsu Bunken Fukyu-Kai: Tokyo, Japan, Sendai, Japan, pp. 208–217.
Orpe, A.V., Khakhar, D.V., 2007. Rheology of surface granular flows. Journal of Fluid Mechanics 571, 1-32.
Parker, D.J., Dijkstra, A.E., Martin, T.W., Seville, J.P.K., 1997. Positron emission particle tracking studies of spherical particle motion in rotating drums. Chemical Engineering Science 52, 2011-2022.
Pignatel, F., Asselin, C., Krieger, L., Christov, I.C., Ottino, J.M., Lueptow, R.M., 2012. Parameters and scalings for dry and immersed granular flowing layers in rotating tumblers. Physical Review E 86, 011304.
Pine, D.J., Weitz, D.A., Chaikin, P.M., Herbolzheimer, E., 1988. Diffusing wave spectroscopy. Physical review letters 60, 1134.
Saw, H.Y., Davies, C.E., Jones, J.R., Brisson, G., Paterson, A.H.J., 2013a. Cohesion of lactose powders at low consolidation stresses. Advanced Powder Technology 24, 796-800.
Saw, H.Y., Davies, C.E., Paterson, A.H.J., Jones, J.R., 2013b. Gas-fluidization and flow properties of fine lactose and mineral powders, in: Kuipers, J.A.M., Mudde, R.F., van Ommen, J.R., Deen, N.G. (Eds.), Fluidization XIV. ECI symposium series, Noordwijkerhout, The Netherlands.
Seiden, G., Thomas, P.J., 2011. Complexity, segregation, and pattern formation in rotating-drum flows. Reviews of Modern Physics 83, 1323.
Seidler, G.T., Martinez, G., Seeley, L.H., Kim, K.H., Behne, E.A., Zaranek, S., Chapman, B.D., Heald, S.M., Brewe, D.L., 2000. Granule-by-granule reconstruction of a sandpile from x-ray microtomography data. Physical Review E 62, 8175.
Tegzes, P., Vicsek, T., Schiffer, P., 2002. Avalanche dynamics in wet granular materials. Physical review letters 89, 094301.
Tegzes, P., Vicsek, T., Schiffer, P., 2003. Development of correlations in the dynamics of wet granular avalanches. Physical Review E 67, 051303.
Tomas, J., 2004. Fundamentals of cohesive powder consolidation and flow. Granular Matter 6, 75-86.
Warr, S., Jacques, G.T.H., Huntley, J.M., 1994. Tracking the translational and rotational motion of granular particles: Use of high-speed photography and image processing. Powder Technology 81, 41-56.
Yamane, K., Nakagawa, M., Altobelli, S.A., Tanaka, T., Tsuji, Y., 1998. Steady particulate flows in a horizontal rotating cylinder. Physics of Fluids (1994-present) 10, 1419-1427.
Yang, H., Li, R., Kong, P., Sun, Q.C., Biggs, M.J., Zivkovic, V., 2015. Avalanche dynamics of granular materials under the slumping regime in a rotating drum as revealed by speckle visibility spectroscopy. Physical Review E 91, 042206.

Zhou, G.G.D., Sun, Q.C., 2013. Three-dimensional numerical study on flow regimes of dry granular flows by DEM. Powder Technology 239, 115-127.
Zivkovic, V., Biggs, M.J., Glass, D.H., Xie, L., 2009. Particle dynamics and granular temperatures in dense fluidized beds as revealed by diffusing wave spectroscopy. Advanced Powder Technology 20, 227-233.